Soft Matter

PAPER

Cite this: *Soft Matter*, 2019, **15**, 3418

Exploring the thermal reversibility and tunability of a low molecular weight gelator using vibrational and electronic spectroscopy and rheology†

David DiGuiseppi,[a] Lavenia Thursch,[b] Nicolas J. Alvarez*[b] and Reinhard Schweitzer-Stenner*[a]

Received 15th January 2019,
Accepted 24th March 2019

DOI: 10.1039/c9sm00104b

rsc.li/soft-matter-journal

Cationic glycylalanylglycine (GAG) self-assembles into a gel in a 55 mol% ethanol/45 mol% water mixture. The gel exhibits a network of crystalline fibrils grown to lengths on a 10^{-4}–10^{-5} m scale (Farrel *et al.*, *Soft Matter*, 2016, **12**, 6096–6110). Rheological data are indicative of a rather strong gel with storage moduli in the 10 kPa regime. Spectroscopic data revealed the existence of two gel phases; one forms below T = 15 °C (phase I) while the other one forms in a temperature range between 15 °C and the melting temperature of *ca.* 35 °C (phase II). We explored the reformation of the cationic GAG gel in 55 mol% ethanol/45 mol% water after thermal annealing by spectroscopic and rheological means. Our data reveal that even a short residence time of 5 minutes in the sol phase at 50 °C produced a delay of the gelation process and a gel of lesser strength. These observations suggest that the residence time at the annealing temperature can be used to adjust the strength of both gel phases. Our spectroscopic data show that the annealing process does not change the chirality of peptide fibrils in the two gel phases and that the initial aggregation state of the reformation process is by far more ordered for phase I than it is for phase II. In the gel phases of GAG/ethanol/water mixtures, ethanol seems to function as a sort of catalyst that enables the self-assembly of the peptide in spite of its low intrinsic propensity for aggregation.

Introduction

Self-assembly of biomolecules is a prominent issue explored in biomedical, biophysical, and bio-material research.[1–7] Understanding how and why certain peptides/proteins prefer to self-assemble into larger networks can reveal the mechanism of amyloid formation and assist in bottom-up designs of supramolecular structures like gels and nanotubes. Over the last ten years, low-molecular weight peptides have emerged as a special class of biomolecules that can self-aggregate into large scale structures like fibrils, colloids, nanotubes and even gels.[2,3,8,9] Hydrogels formed by oligopeptides in (partially) aqueous solutions have multiple beneficial aspects and are potentially useful in biotechnological applications and as tool for developing supramolecular nanostructures.[2] For these reasons, very short, unblocked peptides have become attractive due to their biodegradability, biocompatibility and low production costs.[9–11]

The use of very short peptides that form supramolecular structures was first established by Gazit and coworkers,[12–15] who showed that even unblocked dipeptides, such as diphenylalanine, can self-assemble to form a variety of supramolecular structures, depending on the choice of the solvent. Furthermore, modifications of diphenylalanine, such as the addition of aromatic (fluoroenylmethoxycarbonyl, Fmoc) and aliphatic (*tert*-butyloxycarbonyl, *t*-Boc) end groups considerably increased the propensity for self-assembly.[16,17] The same result can be accomplished by incorporating D-amino acid residues into aromatic tripeptides.[18] These investigations also revealed that adding an aromatic end group to short oligopeptides that are not aromatic can lead to aggregation and even gelation.[13,16,19,20] However, the necessity to add aromatic groups at the N-terminal decreases the peptide's solubility and could increase the costs for any large scale production. One is therefore inclined to identify amino acid sequences of unmodified di- and tripeptides with a high propensity for gelation in aqueous solutions. To this end, Frederix *et al.* worked towards obtaining design rules for a peptide's suitability to form nanostructures under aqueous, pH-neutral conditions.[8,9] They performed MD simulations on all combinations of the twenty common amino acid di- and tripeptides and ranked the resulting peptides by their hydrophobicity and

[a] *Department of Chemistry, Drexel University, Philadelphia, PA 19104, USA. E-mail: rschweitzer-stenner@drexel.edu; Tel: +1-215-895-2268*
[b] *Department of Chemical and Biological Engineering, Drexel University, Philadelphia, PA 19104, USA. E-mail: nja49@drexel.edu; Tel: +1-215-571-4120*

† Electronic supplementary information (ESI) available: Methods, supplementary text, tables and figures. See DOI: 10.1039/c9sm00104b

aggregation propensity. They noted only a weak correlation between the total hydrophilicity of a peptide and its propensity to aggregate. Alanine and glycine were found to exhibit some of the lowest aggregation propensity scores, while the phenylalanine score was by far the highest. Moreover, histidine, in spite of its aromaticity in the deprotonated state, does not have as large of a propensity to aggregate as the other natural aromatic residues F, Y and W.

Recent experiments in our laboratories revealed that the above propensity predictions are not always verified experimentally. Unblocked zwitterionic GHG, for instance, forms hydrogels right upon the deprotonation of its imidazole side chain at centimolar concentrations.[21] Even more surprising was the discovery of Milorey *et al.*,[22] who observed that cationic GAG in 55 mol% ethanol/45 mol% water forms a strong gel at a peptide concentration of 200 mM. Bright field microscopic images revealed that the gel phase of the peptide is underlied by a sample spanning network of crystalline like fibrils on a sub-millimeter length scale. This discovery prompted us to combine a variety of spectroscopic techniques with rheology to probe different steps of the kinetics of the gelation process at different temperatures, to determine the melting temperature of the gel and to characterize different phases of GAG self-aggregation in structural terms.[23] Several surprising results emerged from this study. Vibrational circular dichroism (VCD) spectra revealed the existence of two gel phases formed by peptide fibrils of opposite helicity. A phase with right-handed helical twisted fibrils is formed below 16 °C (phase I), while a network of fibrils with a left-handed twist (phase II) exist between 16 °C and the melting temperature of the gel (28–36 °C, depending on the temperature of formation). Rheological data clearly reveal that the gel of phase I is significantly stronger than that of phase II. We used IR spectroscopy and vibrational and ultraviolet circular dichroism (UVCD) to probe different phases of fibril formation and sample gelation which we found to be related to each other in a highly non-linear manner. Generally, fibrillar structures of even short peptides exhibit a cross β-sheet structure.[13,16,24,25] However, to our surprise, the wavenumber positions of amide I′ bands (′ indicates that D_2O rather than H_2O was used) clearly rule out this possibility. Results from density functional theory (DFT) calculations suggest that GAG oligomers can contain a mixture of peptide adopting β-strand, polyproline II and γ-turn structures.[26] All these results demonstrate that GAG/ethanol/water mixtures stand out among the thus far identified low molecular weight peptide gelators.

In our earlier studies, we very much focused on exploring the thermal stability of the obtained gel phases and the complex kinetics of their formation processes. Some experiments revealed a hysteresis for the melting of both phases, which indicates that the melting process is not fully thermoreversible.[23] While the reversibility of short peptide gels under different forms of stress has attracted some attention,[25,27,28] the thermoreversibility of peptide gels has been only sporadically investigated.[29] However, it is of utmost importance for the technical applicability of gels and for a thorough understanding of the respective gelation process. There are many applications that would require a gel to be fully reversible such as biosensors and some drug release systems;[30] while non-reversibility might allow for an adjustment of gel properties for other applications such as topical ointments.[31]

The current study is aimed at closing this gap for cationic GAG in ethanol/water. We used spectroscopic techniques and rheology to determine (a) to what extent gel formation is delayed as a function of the time the sample stays at 50 °C and (b) whether or not reformation yields gels of the same strength and structure of the underlying fibrils. Our results clearly show that both gelation phases represent metastable states and the strength of the gels can be adjusted to a desired value by choosing the appropriate annealing time. Neither of the gelation phases are formed if the sample is allowed to stay at high temperatures for a longer period of time.

Materials and methods

Materials

Unblocked glycyl-alanyl-glycine (H-Gly-Ala-Gly-OH) was purchased from Bachem with >99% purity and used without further purification. Solvent mixtures of 55 mol% ethanol (200 proof, Pharmco-Aaper)/45 mol% deionized water were used to prepare the gel samples. Deuterated solvents, D_2O (99.9% purity, Sigma Aldrich) and ethan(ol)-d (EtOD, 99.9% purity, Sigma Aldrich), were used for the vibrational spectroscopy studies to avoid the overlap of the strong water band at 1640 cm^{-1} with the amide I region (1600–1700 cm^{-1}). EtOD is the deuterated ethyl alcohol with the alcoholic hydrogen replaced by deuterium. The pH of the samples was adjusted to about 2 by adding HCl (ACS grade, Ricca Chemical Company) to ensure complete protonation of GAG.

Ultra-violet electronic circular dichroism (UVCD) and absorption

Spectra were measured on a Jasco J-810 spectropolarimeter (model J-810-150S) purged with nitrogen. The temperature was controlled using a Peltier controller (model PTC-423S). The sample was loaded onto a 100 μm cell from International Crystal Laboratories. UVCD spectra were recorded between 180 and 300 nm with a 500 nm min^{-1} scan speed, 1 s response time, 0.05 data pitch, and 5 nm bandwidth. Five spectra were obtained and averaged at each time interval, and all spectra were corrected using appropriate background subtraction. Absorption spectra were obtained simultaneously with the CD spectra. For the annealing cycles, heating and cooling to and from the annealing temperature of 50 °C took between 2.5 to 3 minutes and 3.5 to 5 minutes, respectively.

Vibrational circular dichroism and Fourier transform infrared (VCD/FTIR) spectroscopy

As described above, vibrational spectroscopy studies required the use of deuterated solvents. IR and VCD spectra were measured on a BioTools ChiralIR and were loaded in a 121 μm CaF_2 biocell from Biotools. Spectra with a resolution of 8 cm^{-1} and scan speed of 83 scans per minute were collected using the Grams/IR 7.00 software (Thermo Galactic). For kinetics studies, two minute scans

were collected every five minutes for the desired length of time. For steady state measurements, ten hours scans were collected. The temperature of the sample was maintained by a BioTools water-cooled temperature controller. The IR spectra were not solvent corrected in order to allow us to observe any changes of the solvent bands. Part of the observed spectra were decomposed into individual Gaussian bands using our MULTIFIT program.[32] For the annealing cycles heating and cooling to and from the annealing temperature of 50 °C took between 2.5–3 minutes and 2–3 minutes, respectively.

Rheology

Rheology measurements were obtained on a DHR-3 (TA instruments) using a Peltier plate for temperature control with a top plate of diameter 25 mm. 500 to 600 μL of peptide material was used. To avoid solvent evaporation, safflower oil was added to the top of the upper plate, to act as a solvent trap. The ethanol/water solutions were confirmed to have little to no solubility in the oil phase. All samples were prepared two to four minutes prior to loading onto the Peltier plate. The exact time between ethanol addition and beginning of the experiment was recorded and accounted for during data treatment. A strain percent of 0.03%, an angular frequency of 1 rad s^{-1}, and a gap of 700 μm were used for the small amplitude oscillatory shear measurements. The storage and loss moduli as well as the tan δ were recorded as a function of time. The moduli during initial formation at either 5 °C or 20 °C were recorded over a period of 5800 seconds. The sample was then brought to 50 °C at a rate of 15 °C per min, held at 50 °C for 5 min, brought back to 5 °C or 20 °C at a rate 15 °C per min and then incubated for 5800 seconds while recording modulus. This cycle was repeated twice for the 5 °C → 50 °C → 5 °C and the 20 °C → 50 °C → 20 °C annealing cycle.

Microscopy

Microscopy experiments were performed on a Nikon Eclipse TE2000-S inverted microscope using the 4×/0.13 Nikon Plan Fluor lens. The peptide gel sample was prepared 24 h in advance at room temperature in a closed glass cell equipped with a thermocouple. After this incubation time, the cell was held at 50 °C for 5 min. The video recording was then started as the sample was cooled to room temperature. One frame was captured every minute over the span of two and a half hours. For monitoring the melting of the gel, the temperature was increased with a rate of 0.66 °C min^{-1}, the cooling rate was −9 °C min^{-1}. Thus, the cooling step for reformation at 23 °C lasted 3 minutes.

Results and discussion

This chapter is organized as follows. We will first demonstrate that neither phase I (formed at 5 °C) nor phase II (formed at 20 °C) GAG gels are formed after annealing the sample over a period of 16 h at 50 °C. Next, we will show how rheology, electronic and vibrationally spectroscopy reveal the dynamics of gel reformation after short annealing times. The obtained information about the kinetics of different reaction steps will then be utilized for descriptions of the reformation of the gel phases I and II.

Sixteen hour annealing at 50 °C

We first investigate the reversibility of gel formation of GAG in 55 mol% ethanol/45 mol% water after melting, annealing, and subsequent cooling. The sample was held at 50 °C for sixteen hours to ensure steady state prior to the cooling of the sample. Typically, one would observe a cloudy gel like solution if the solution is made at temperatures below 25 °C. However, the heated solution showed no observable gelation even several days after cooling. This observation suggests that the previously reported gel phases are kinetically trapped, meta-stable states which do not represent a thermodynamic equilibrium. Apparently, upon melting at elevated temperatures peptides fibrils underlying the gel phase dissociate into either monomers or short disordered oligomers that do not reform into fibrils. We employ ECD, IR, and VCD spectra to explore the corresponding conformational changes.

Fig. 1 compares the ECD, IR and VCD spectra of: (left) the gel after initial formation at 20 °C and 5 °C, (middle) after annealing the sample at 50 °C for 16 hours, and (right) after subsequently cooling the annealed sample to 20 °C and 5 °C. The left column of Fig. 1 shows clearly the observed signatures of GAG self-assembled into fribils in all of the recorded spectra. The UVCD spectrum has been shown earlier to probe a late phase of peptide fibrilization which often but not always precedes gelation. The observed dichroism is most likely caused by the increasing anisotropy of the fibrillar network,[33] as shown in microscopic images (Fig. 2). For both gel phases, the UV spectrum exhibits an intense positive maximum at *ca.* 215 nm with a more pronounced signal for phase I. The IR spectra of the two phases display a splitting of the amide I′ band which is indicative of the formation of at least somewhat ordered oligomers and filaments.[26] The corresponding VCD spectra reflect the formation of two distinct left (phase II, T = 23 °C) and right handed chiral structures (phase I, T = 5 °C) depending on the temperature of formation.[34–36]

The spectra in the middle column reflect drastic changes after annealing phase II at 50 °C for 16 hours. Microscopic images show that the fibrils begin to visibly disappear upon heating above 27 °C and are nonexistent at 40 °C (Fig. 2). Correspondingly, the positive maximum at 215 nm in the UVCD spectrum is replaced by a shallow negative maximum. The split amide I′ bands are merged into one broad band, similar to what we observed earlier for GAG monomers in 40 mol% ethanol/60 mol% water.[22,37] The corresponding VCD signal is more than an order of magnitude weaker than those of both gel phases and very negatively biased; suggesting the absence of any long-range order. However, it is still a factor of 3 more intense than the corresponding VCD of the monomer.[37] This signal could suggest a racemic mixture of short left- and right handed oligomers. The existence of peptide oligomers is further corroborated by the respective UV absorption spectra in Fig. S1 (ESI†), which were recorded as a function of time and for different thermal histories. Apparently, the absorption spectrum does not return to that of

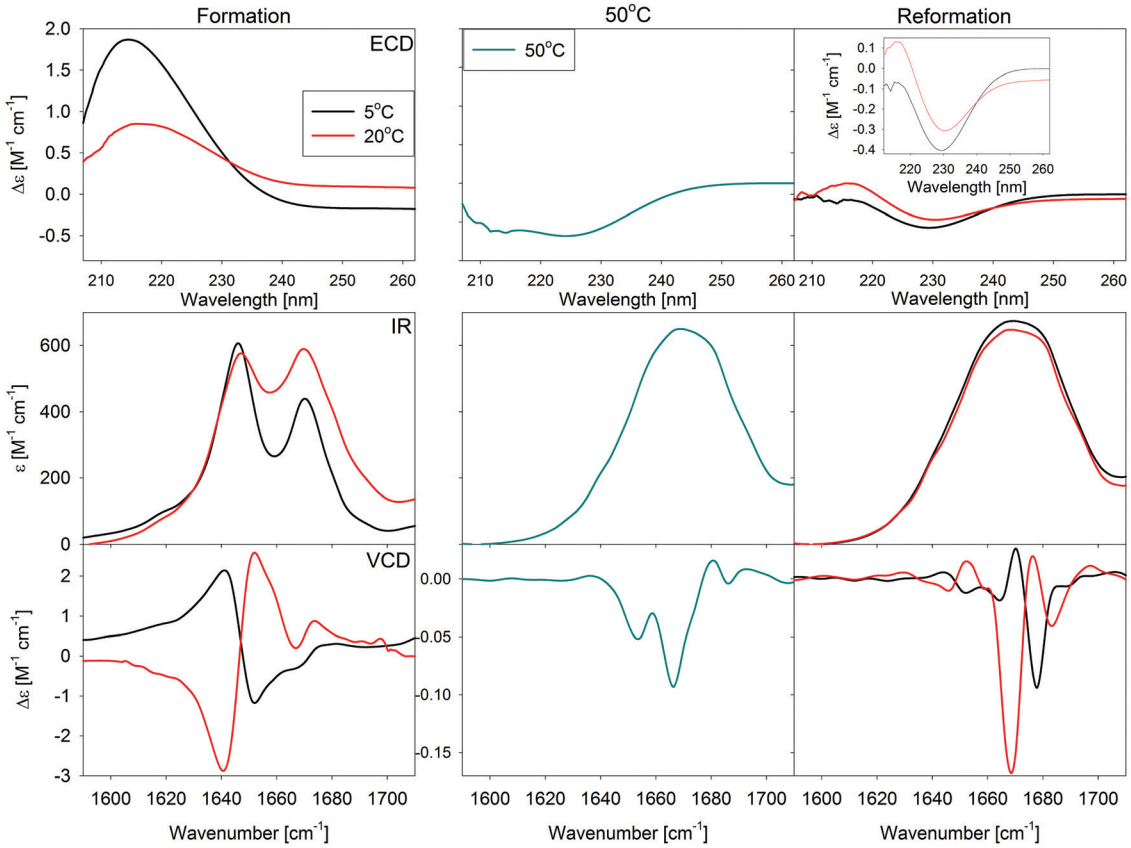

Fig. 1 ECD (top), IR (middle) and VCD (bottom) spectra of ternary GAG/ethanol/water mixtures after initial formation (left), after being held at 50 °C for sixteen hours (middle) and after subsequently cooled down to lower temperatures (right). The inset is added for clarity regarding the shape of the signals. The GAG concentration the mol% values of ethanol and water and given in the Material and methods section.

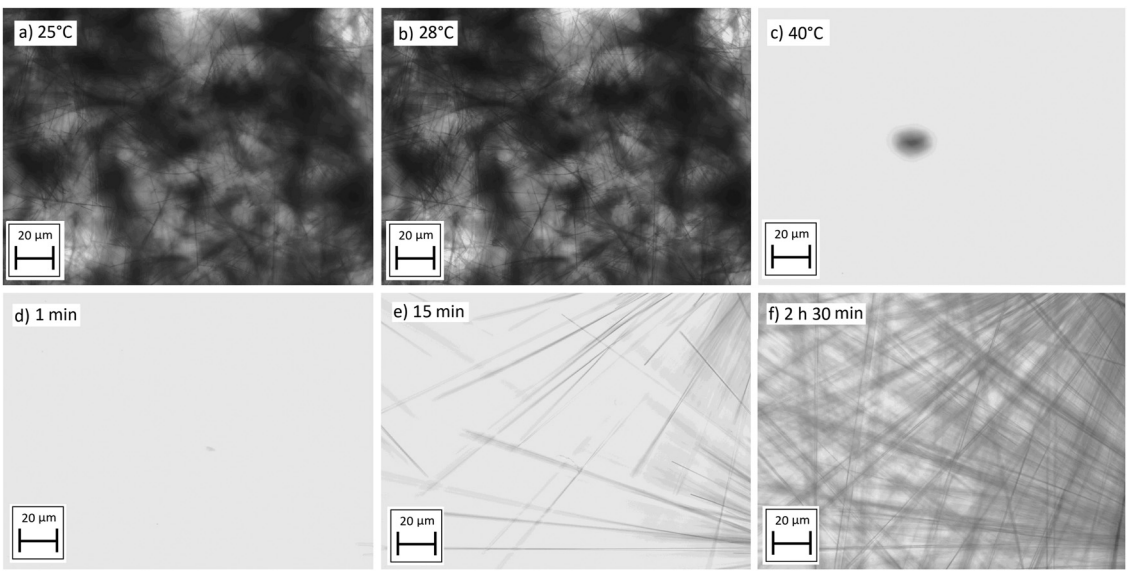

Fig. 2 Micrographs from video captures of the GAG melting and reformation. The top row images are captures of GAG during melting process at (a) 25 °C, (b) 28 °C, (c) 50 °C. The bottom row shows pictures after a 20 °C → 50 °C → 20 °C annealing cycle. The images were taken (d) 1 min, (e) 15 min, (f) 2 h 30 min after completing the annealing cycle.

the peptide monomer. Instead, it quickly reaches a steady state signature that shows differences and similarities to and with the original gel. While the spectrum of the monomer exhibits the canonical NV1 band at 185 nm, which is generally assigned to a

HOMO → LUMO transition of the peptide groups,[38] the spectra of the gel phases as well as those measured during and after the annealing processes depict two bands at 195 and 210 nm. The authors are not aware of any such recorded redshift for simple peptides like GAG. Overall the data indicates that at high temperature the peptides are still assembled oligomers which, as we will see below, do not have the capability to seed long range fibrilization and gelation.

The right column shows the spectra of a sample that had been cooled from 50 °C to 5 °C (phase I) and 20 °C (phase II). The cooled samples scattered no light and showed no signs of fibrils in the microscope (data not shown). At first glance, the spectra of the cooled samples seem to be very similar spectra in UVCD, IR, and VCD to the heated samples at 50 °C. While this is undoubtedly true for the IR absorbance spectrum, there are key differences in the UVCD and VCD spectra which are reminiscent of the initial gel spectra, namely the positive maximum in the UVCD spectrum at 215 nm in the spectrum recorded at 5 °C and (ii) the return of the negative amide I′ couplet at 20 °C and of a positive one at 5 °C. The latter are still much weaker than the corresponding signals of the gel phase. The ECD spectrum seem to suggest that the molecules have formed a β-strand/sheet like structure with the positive and negative maxima redshifted from the canonical positions (195 and 215 nm, respectively).[39] Regardless of β-strand/sheet formation, it is clear that the UVCD and VCD spectra suggest the presence of peptide aggregates that are different than the oligomers observed at 50 °C.

Taken together, these results clearly indicate that upon incubation of cationic GAG in binary mixtures of ethanol and water the peptides quickly self-aggregate into chiral oligomers that grow into helically twisted filaments which subsequently form macroscopic fibrils provided that peptide concentration and ethanol fraction exceed certain critical values. Recently we provided experimental evidence for a scenario where GAG accumulates at ethanol/water interfaces with the protonated C-terminal peptide group immersed in ethanol while the N-terminal peptide group is still exposed to water.[40] Thus, ethanol could 'catalyze' the self-assembly of the peptide. The respective fibrils form the sample spanning network of the gel phases. When the fibrils are melted and held at elevated temperatures (in this case 50 °C) they rearrange to form oligomeric structures that when cooled regain chirality, but do not self-assemble into macroscopic moieties. These observations show that the gels are not reversible structures and rather represent a kinetically trapped, meta-stable state due to the subcooled nature of the sample.

While the above results show that the gel cannot be reformed after staying for a long residence time at elevated temperatures, it is very likely that gelation can occur if the residence time is short. Our earlier results suggest that gels can reform if the residence time is on the order of minute.[23] Below, we explore in more detail the reformation after short annealing processes with regard to its initial and final temperature.

Annealing and gel reformation

The experiments described below were designed to explore how the kinetics of self-aggregation and gelation as well as the strength of the reformed gel are affected by the residence time at 50 °C. We start with observations from microscopy, proceed to rheological measurements which directly probe the dynamics of gel formation, and then focus the kinetics of pre-gelation processes *via* spectroscopic methods. While the rheological measurements run through several annealing cycles, the spectroscopic measurements were performed to elucidate the mechanism of a single reformation process.

Microscopy/videos. In an attempt to visually observe the fibrils without the use of spectroscopic or rheology techniques, we formed the gel on a custom closed microscope slide setup at room temperature and heated it up to 50 °C, the sample was then cooled to 20 °C and the reformation process was recorded. Some snapshots of the reformation process are shown in Fig. 2. A video of the process is available ESI.† Initially off screen, we observe the formation of a nucleus center, with needles protruding radially in all directions. At a later time, these needles grow in length and additional needles appear. At a critical time, the needles overlap and form the sample spanning network that denotes the observed gel phase II. The length of most fibrils extends into the millimeter range and have a flat sheetlike shape with a width of ∼1–5 μm. Corresponding images of the initial gel formation process in Farrell *et al.* reveal a much denser final network (*cf.* also the upper left image in Fig. 2). From these images we expect that the reformed phase II gel should be of reduced strength compared with that formed directly at 20 °C.

Rheology. We directly probed the kinetics of re-gelation after annealing phase I and II gels at 50 °C for 5 min intervals and subsequently cooling each of the sample to either 5 °C or 20 °C. The annealing cycles involving solely phase I (5 °C → 50 °C → 5 °C) or phase II (20 °C → 50 °C → 20 °C) were repeated twice. The respective kinetic traces of the storage modulus (G') are shown in Fig. 3. The corresponding plots of the loss moduli (G'') are shown in Fig. S2 (ESI†). Fig. 3a and b compare the kinetics of phase I and II formation and of their respective reformation after a single annealing cycle. In addition, Fig. 3c and d show the kinetic traces for the initial formation at 5 °C (phase I) and 20 °C (phase II), respectively, together with the respective kinetic traces obtained after repeated annealing processes. Note that based on their high G' values the initially formed gel, particularly that of phase I, are considerably strong gels when compared to typical peptide hydrogels reported in literature for which the G' values lie generally in the 10^3–10^4 Pa region.[5,13,17,25,27,29,41,42]

Farrell *et al.* analyzed the kinetic traces of the storage and loss modulus of GAG-gelation by fitting a model by Gao *et al.* to their experimental data.[23,43] The respective equation can be understood as a linear combination of two stretched exponentials that represent different inhomogeneous relaxation processes. Here, we employ a somewhat more simplistic and heuristic model which just accounts for sigmoidal character of the kinetic traces in Fig. 3. The corresponding equation for the storage modulus is written as:

$$G' = \frac{G_{\max}{}'}{1 + \left(\frac{t}{\tau}\right)^a} \quad (1)$$

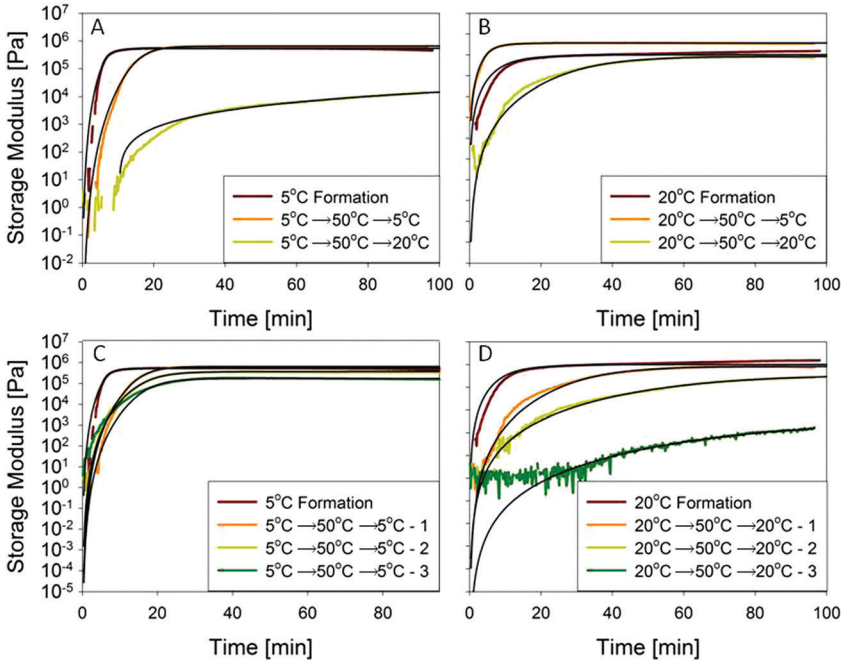

Fig. 3 (A) Storage modulus obtained by rheology for samples formed at 5 °C and of samples reformed at indicated temperatures; (B) storage modulus obtained by rheology for samples formed at 5 °C and for samples reformed at indicated temperatures; bottom: storage modulus obtained by rheology for samples formed at 5 °C (C) and 20 °C (D) depicted together with the corresponding storage moduli obtained after multiple annealing cycles. The solid lines result from fits of eqn (1) to the data described in the paper.

where G_{max}' is the maximal storage modulus reached when the kinetic trace levels off, τ is an effective time constant given by the inflection point of the trace and the constant a can be interpreted as a measure of the cooperativity of the gelation process. Eqn (1) was fitted to the kinetic traces in Fig. 3 by using a non-linear least square routine. The parameters and the corresponding statistical errors obtained from fitting eqn (1) to the experimental data in Fig. 3 are listed in Table 1.

The kinetic traces in Fig. 3a show that the formation and reformation of phase I at 5 °C (5 °C → 50 °C → 5 °C) result in a gel with a similar connectivity where the G_{max}'-value solely decreases from 539 to 172 kPa (Table 1). However, the 5 °C → 50 °C → 5 °C reformation proceeded on a slower time scale than the formation after the second and even more so after the third annealing cycle (*cf.* the τ-values in Table 1). The same can be said about the annealing cycle involving a phase II to phase I transition (20 °C → 50 °C → 20 °C). The kinetic traces in Fig. 3 and our analysis showed that the reformation after the completion of the annealing cycles that ended at 20 °C (20 °C → 50 °C → 20 °C and 5 °C → 50 °C → 20 °C) proceeded substantially slower than the corresponding phase I reformation (*cf.* τ-values in Table 1). Moreover, the repeated 20 °C → 50 °C → 20 °C annealing cycles lead to a substantial decrease of G_{max}' from 172 kPa after initial formation to nearly 300 Pa after the 3rd annealing cycle. Reformation after the phase I → phase II process proceeded even slower and did not reach the final value in the investigated time window. From our fit we obtained a G_{max}' value of 147 kPa, which lies below the respective value for phase II formation and is considerably lower than the corresponding value for phase I reformation (659 kPa). Interestingly, the obtained negative a-values suggest that overall the investigated reformation processes are little bit more cooperative than the respective formation processes (Table 1).

Since the lack of reproducibility is known to frequently ensnare the experimental work exploring the self-assembly of

Table 1 Parameter values obtained from fitting eqn (1) to the gelation kinetics depicted in Fig. 1

Trial	G_{max}' [kPa]	τ [min]	a	R^2
5 °C formation	539 ± 2	7.15 ± 0.02	−4.84 ± 0.02	0.99
5 °C → 50 °C → 5 °C #1	659 ± 2	17.74 ± 0.02	−5.99 ± 0.02	0.99
5 °C → 50 °C → 5 °C #2	379 ± 2	19.73 ± 0.03	−4.9 ± 0.02	0.99
5 °C → 50 °C → 5 °C #3	172 ± 5	20.0 ± 0.1	−5.73 ± 0.02	0.98
20 °C → 50 °C → 5 °C	374 ± 6	6.57 ± 0.02	−3.03 ± 0.02	0.98
20 °C formation	172 ± 25	29.13 ± 0.7	−1.38 ± 0.03	0.99
20 °C → 50 °C → 20 °C #1	83.9 ± 0.4	40 ± 0.2	−4.42 ± 0.07	0.99
20 °C → 50 °C → 20 °C #2	39.6 ± 0.3	75.5 ± 0.4	−3.55 ± 0.02	0.99
20 °C → 50 °C → 20 °C #3	0.351 ± 0.03	103.4 ± 3	−3.82 ± 0.09	0.99
5 °C → 50 °C → 20 °C	147 ± 92	360 ± 88	−1.77 ± 0.04	0.99

peptides or proteins we repeated the measurements of phase I and II reformation kinetics after subsequent annealing cycles. Fig. S3 (ESI†) compares the respective kinetics traces. From the fits of eqn (1) to these traces we found that the corresponding parameter values for both trials (*i.e.* G_{max}', τ and a) differ by less than 20% for the phase I gels. For the reformation of the phase II samples, the differences in parameter values are larger, *i.e.* between 5% and 35%. As shown below, the reformation at 20 °C is subject to instabilities which might make it more difficult to reproduce the rheology kinetics. However, the obtained uncertainty does not obfuscate the general trend of how repeated annealing processes reduce G_{max}' and increase τ (Fig. S3, ESI†).

Three important points can be made based on our experimental findings: (1) the strength of the gel is always higher for phase I reformation at 5 °C regardless of initial formation temperature, (2) the strength of the reformed gel depends to a predominant extent on the reformation temperature and (3) the reformation gelation kinetics are slower than initial formation and faster at 5 °C than it is at 20 °C. We hypothesize that (1) is due to dissociation of peptide fibrils into non-fibril forming oligomers at elevated temperatures, (2) is due to the type of fibril that is formed at different temperatures, and (3) less peptide oligomers available to form fibrils means slower kinetics and subcooling the peptide solution to 5 °C induces faster fibril formation kinetics. These results clearly indicate that the gel's fibril microstructure can be readily tuned by the annealing time at elevated temperatures and by the subcooled reformation temperature.

The hypothesis of a dynamic transition of fibril forming oligomers into non-fibril forming oligomers is supported by the results of the 16 h annealing experiment as well as by the rheology kinetics depicted in Fig. 3c and d, which represent gel structure after repeated annealing cycles. The depicted kinetic traces indicate a decrease in the rate of fibril formation (as reflected by increasing τ-values in Table 1) and the strength of the gel with the 2nd and 3rd repetition. Both changes are much more pronounced for the reformation kinetics of phase II.

Since the storage modulus is proportional to the density of percolated fibrils, our data suggests that the number of fibrils are decreasing with annealing time at 50 °C. This conclusion, which is corroborated by microscopic images (Fig. 2) strongly suggests that there is a dynamic transition of peptide oligomers to non-fibril forming structures at 50 °C. This transition appears to happen quite quickly since after three cycles (15 min at 50 °C) very few peptide oligomers are left to form a dense volume spanning percolated network.

It deserves to be noted that the tan δ values of the formation and reformation processes differ (Fig. S4, ESI† and Table 2) in that they are lower for the latter. This suggest that reformation actually leads to a more normal gel phase where G' substantially exceeds G''.

Finally, some differences between the rheology data in this and our former study should be acknowledged.[23] A frequency sweep yielded G'-values in the range of 20 kPa for phase II, which is substantially lower than the G_{max}' value obtained in this study (Table 1). Moreover, the kinetic traces reported by Farrell *et al.* indicate a much slower formation kinetics. However, this and our study still convey the same message by indicating that the phase I gel is stronger and more stable than the phase II gel. A large number of rheology experiments performed in our laboratory led us to the conclusion that great care has to be taken to ensure that experiments are performed with samples of identical pH and ionic strength and that any evaporation of ethanol is avoided. These conditions are met by the studies reported in this paper.

Table 2 tan δ values of gel phases obtained after initial formation and different annealing processes obtained from the G_{max}' and G_{max}'' values of the gelation kinetics shown in Fig. 3 and Fig. S2 (ESI)

Sample	tan(δ)	Sample	tan(δ)
5 °C formation	0.401	20 °C formation	0.394
5 °C reformation	0.258	5 °C reformation	0.227
20 °C reformation	0.353	20 °C reformation	0.454
5 °C 1st reformation	0.258	20 °C 1st reformation	0.454
2nd reformation	0.270	2nd reformation	0.277
3rd reformation	0.275	3rd reformation	0.353

UVCD spectroscopy. Fig. 4a shows the kinetics of GAG fibrillization probed by changes of the UV circular dichroism at 221 nm for initial formation at 20 °C and for the reformation after annealing at 50 °C for three and five minutes and cooling to a specified temperature. The solid lines represent fits to the data with a model described below. Two observations are notable. First, the kinetic traces of reformation indicate a lag time not observed in the CD-kinetics of the initial gel formation where the $\Delta\varepsilon_{221}$ signal increases without any visible lag time for both gel phases.[23] A retardation of the UVCD formation kinetics was observed only in a narrow temperature interval between 14 °C and 17 °C. We observed that the $\Delta\varepsilon_{221}$ amplitude observed after reaching a steady state is generally weaker for all reformed samples than it is observed for the initial formation. Only for reformation at 5 °C does $\Delta\varepsilon_{221}$ reach the magnitude of the initial formation kinetics at 20 °C very much *in sync* with the results of the corresponding rheology experiments. Fig. 4b shows the kinetics of the $\Delta\varepsilon_{221}$ response at 5 °C and 20 °C after completion of the annealing cycles 5 °C → 50 °C (5 min) → 5 °C and 5 °C → 50 °C (5 min) → 20 °C. While the former re-establishes the original $\Delta\varepsilon_{221}$ values after a lag time of *ca.* 15 minutes, the amplitude of the latter is considerably lower while the respective lag time is longer. These observations and earlier results[23] strongly suggest a close correlation between the final values for the storage modulus and $\Delta\varepsilon_{221}$.

As for our rheological experiments, we checked the reproducibility of the CD kinetics. In view of the time required for each experiments, we repeated only the phase 1 annealing cycle experiment three times. The exposure time at 50 °C was again five minutes (Fig. S5, ESI†). While the kinetic traces do not completely overlap the kinetic trends are the same and the overall difference between the amplitudes is less than 0.1 M^{-1} cm^{-1}. Hence, we can conclude that the reproducibility of the CD kinetics is more than sufficient for the purpose of this study.

Farrell *et al.*[23] subjected the $\Delta\varepsilon_{221}$ kinetic traces of initial gel formation to an analysis which was based on the aggregation model of Knowles *et al.*[44] It considers the growth of nuclei as

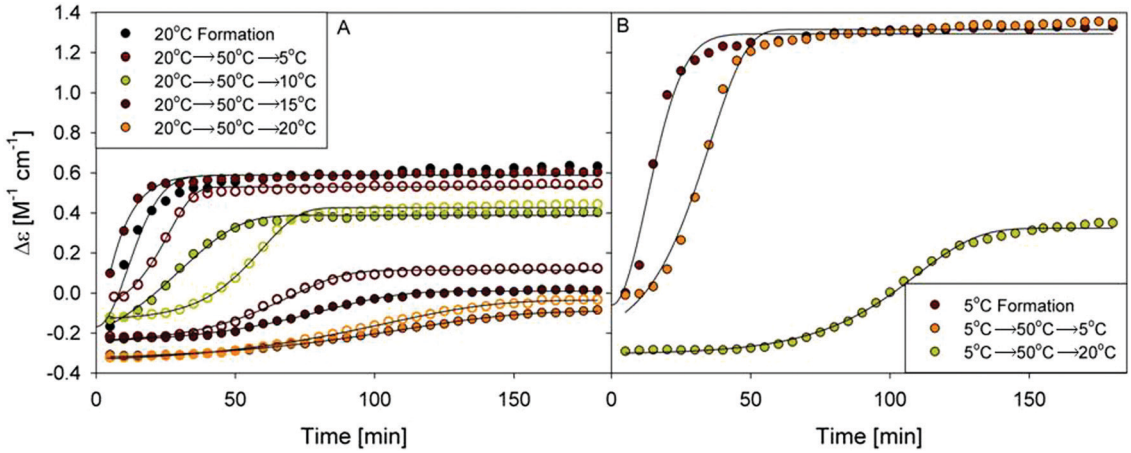

Fig. 4 UV circular dichroism of 220 mM GAG in 55 mol% ethanol/45 mol% H_2O monitored at 221 nm as a function of time after formation and reformation at indicated temperatures. (A) All gels were formed at 20 °C (black dots) and reformed at the indicated temperatures. Kinetic reformation traces of samples held at 50 °C for three and five minutes are displayed by open circles and closed circles, respectively. (B) All gels were formed at 5 °C (black) and reformed at 5 °C (orange) and 20 °C (green).

well as a second nucleation processes caused by the dissociation of fibrils. Assuming that $\Delta\varepsilon_{221}$ is a measure of the mass concentration of filaments, Farrell *et al.* arrived at the following formalism:[23]

$$\Delta\varepsilon_{221}(t) = A\left[1 - \exp\left(-\left(B_+ + \frac{C}{2}\right)e^{\kappa t} + \left(B_- - \frac{C}{2}\right)B_- e^{-\kappa t} + C\right)\right] + \Delta\varepsilon^0_{221}(t) \quad (2)$$

A is a scaling factor proportional to the total peptide concentration. The coefficients $B_\pm$ are defined as follows:

$$B_\pm = \frac{k_+}{k}P(0) \pm \frac{M(0)}{2m_{\mathrm{tot}}} \quad (3)$$

where $P(0)$ and $M(0)$ are the initial number and mass concentrations of the filaments. For the fits to the initial formation kinetics, we assumed that $B_\pm$ = 0. The coefficient C can be written as:

$$C = k_n m_{\mathrm{tot}}^{n_c-1} k_-^{-1} \quad (4)$$

The rate constant κ is written as:

$$\kappa = \sqrt{2m_{\mathrm{tot}}k_+k_-} \quad (5)$$

where k_+ is the rate constant for monomer addition to a peptide polymer, k_- is the corresponding dissociation constant, k_n is the nucleation rate constant and m_{tot} is the total concentration of peptides. The theory of Knowles *et al.* is a simplification since it does not consider intermediates associated with conformational changes of the protein and by design, it does not account for the crosslinking of fibrils.[44] However, if the latter exhibits a linear relationship with the mass concentration of filaments, the entire approach is well suited for describing a process that precedes crosslinking and gelation.

Eqn (2) was fitted to the reformation kinetic traces in Fig. 4a and b. In view of the simplicity of the theory we consider the agreement with experimental data as satisfactory. The fitting parameters are listed in Table 3. Some aspects of these parameters are noteworthy. The parameter κ appears in a cosh-type function in the argument of the exponential function in eqn (2), if it increases the negative value of the argument, a more rapid

Table 3 Parameter value obtained from fitting eqn (2) to the UVCD kinetics depicted in Fig. 4 for samples formed at 20 °C, held at 50 °C for three minutes and reformed at the indicated temp (top), formed at 20 °C, held at 50 °C for five minutes and reformed at the indicated temp (middle), and formed at 5 °C, held at 50 °C for five minutes and reformed at the indicated temp (bottom)

T [°C]	A	κ [min^{-1}]	C	$\Delta\varepsilon_{221}$ [M^{-1} cm^{-1}]	B	R^2	Std. error
5	0.49	0.13	0.58	0.10	0.01	0.97	1.78×10^{-2}
10	0.47	4.8×10^{-2}	0.44	−0.083	0.01	0.97	1.29×10^{-2}
15	0.24	3.7×10^{-2}	8.2×10^{-2}	−0.23	0.01	0.97	0.68×10^{-2}
20	0.22	2.4×10^{-2}	0.12	−0.31	0.01	0.99	0.39×10^{-2}
5	0.57	0.11	0.11	−0.040	2.5×10^{-3}	0.97	1.23×10^{-2}
10	0.55	7.5×10^{-2}	1.8×10^{-2}	−0.16	2.5×10^{-3}	0.97	1.23×10^{-2}
15	0.34	5.0×10^{-2}	5.7×10^{-2}	−0.23	2.5×10^{-3}	0.97	1.03×10^{-2}
20	0.28	2.6×10^{-2}	0.13	−0.31	2.5×10^{-3}	0.98	0.44×10^{-2}
5	1.39	0.07	0.12	−0.075	2.5×10^{-3}	0.97	4.01×10^{-2}
20	0.62	4.6×10^{-2}	7.9×10^{-3}	−0.30	2.5×10^{-3}	0.97	1.48×10^{-2}

increase of the $\Delta\varepsilon_{221}$ is produced. Therefore, its increase with decreasing cooling temperature makes sense. The *B*-values account for the fact that some initial filament concentration must exist, but the reported values carry a large uncertainty. The *C*-parameter is in the argument of the exponential function of eqn (2) and thus determines the effective time constant of the kinetic process to a significant extent. Its low values (compared with corresponding values reported by Farrell *et al.*) lead to the observed lag times and a more pronounced sigmoidal behavior. Its dependence on the cooling temperature is non-monotonous, which might be due to the crossover between different gel phases.[23] It exhibits the lowest value for a cooling temperature of 15 °C for the 3 minutes cycle and of 10 °C for the 5 minutes cycle which corresponds to the most sigmoidal curves of the respective data sets.

As indicated above the relationship between the fitting parameter *C* and the total peptide concentration is described by a power law (*i.e.* the term $m_{\mathrm{tot}}^{n_c-1}$). Depending on the value of n_c the value of *C* can vary significantly even for small variations of m_{tot}. A comparison of the *C*-values obtained for the reformation process (*cf.* Farrel *et al.*[23]) and the values in Table 3 reveal that the latter are between 4 and 5 orders of magnitude lower than those reported for the former. In our case m_{tot} is likely to represent the peptides that are still not digested by off-pathway aggregation (*vide supra*). If we assume that the concentration of peptide still available for fibrilization is just one tenth of the original peptide concentration, a nucleation number n_c of 5 or 6 could easily explain the enormous drop of *C*-value after annealing. However, a closer look at the κ-values suggest that kinetic parameters of formation and reformation might be somewhat different. If only m_{tot} changes during the annealing process the value for κ should decrease (approximately by a factor of 3 for the above scenario). A comparison of the κ-values in Table 3 and those reported for the gel formation reveal that the reformation values are actually larger. That could reflect a larger k_- value for the latter, which would result in an additional decrease of *C* (eqn (3) and (4)). A larger k_- value would indicate that filaments are less stable after reformation.

VCD and IR spectroscopy. Various research groups have reported over the last ten years that vibrational circular dichroism (VCD) can be used to study fibril formation.[34–36] Generally, peptide fibrils are built with cross β-sheet tapes that adopt a helical twist. Owing to considerable length of the structure, this twisting enhances the otherwise weak VCD signal of amide I modes since it is mostly produced by excitonic coupling between oscillators in adjacent strands.[36,53] Our earlier reported amide I′ profiles in the IR and VCD spectra of GAG gels suggest that a twisting of less ordered sheets that do not exhibit the canonical β-sheet structure can still lead to a substantial enhancement of the VCD signal.[26] Concomitantly, we observe a splitting of the amide I′ profile in the IR spectrum (*vide supra*). Both the VCD enhancement and the IR band splitting reflect a delocalization of amide I modes due to interstrand excitonic coupling. If the degree of structural order is high and if the twisting of filaments/fibrils is homogeneous, intensity in the IR and VCD spectrum is dominated by a few transitions into excitonic states.[36]

We have used the VCD signal of amide I′ together with the corresponding IR spectra to track the reformation kinetics of the GAG filaments/fibrils in ethanol/water over time. In Fig. 5, we present spectra for annealing cycles with initial formation at 5 °C and 20 °C, annealing at 50 °C for five minutes, and ending at 5 °C and 20 °C (additional spectra are reported in Fig. S6–S9, ESI†).

The following observations are particularly noteworthy. First, the amide I′ VCD signal strength of the sample produced by the 5 °C → 50 °C → 5 °C cycle is almost an order of magnitude larger than that of the initially formed gel at 5 °C. This observation is remarkable since the phase I gel initially formed at this temperature already shows a signal strength two orders of magnitude larger than that of monomeric GAG in solution. While the amplitudes are different, the signs of the signals (positive couplet) are identical, which suggests a similar helix-like twisting after reformation. Contrary to this observation,

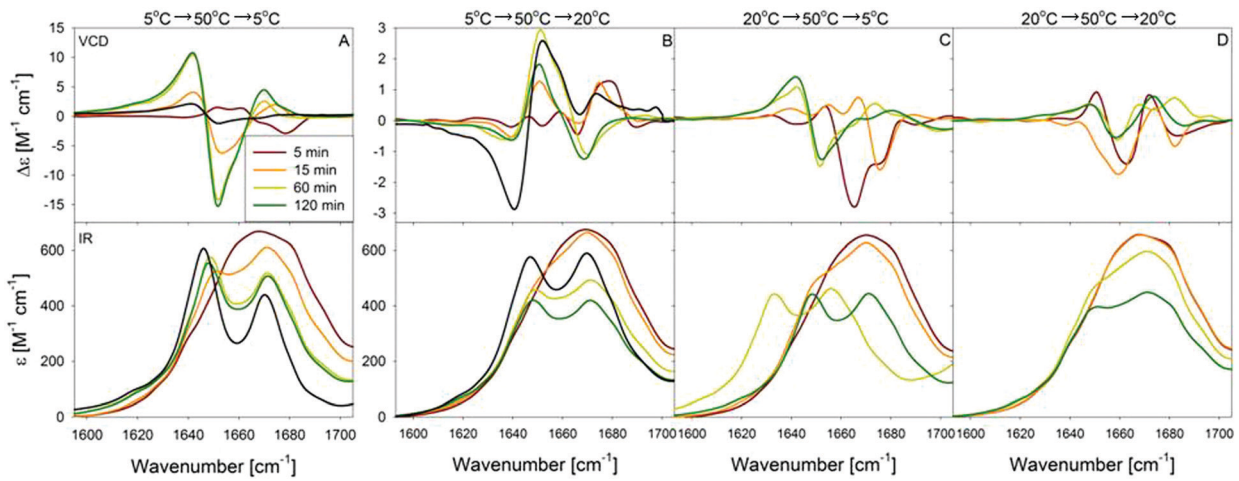

Fig. 5 VCD and IR spectra recorded during the reformation process of ternary GAG/ethanol/water samples (A) formed at 5 °C and reformed at 5 °C, (B) formed at 5 °C and reformed at 20 °C, (C) formed at 20 °C and reformed at 5 °C, and (D) formed at 20 °C and reformed at 20 °C. The bolded spectra in A and B are the spectra of the initially formed samples at 5 °C (A) and 20 °C (B) at the respective temperatures. All reformed samples were held at 50 °C for 5 min.

the 20 °C → 50 °C → 5 °C cycle produces a positive couplet that is comparable in magnitude with the initial gel formed at 20 °C. The VCD of amide I′ showed a very peculiar behavior after the two annealing cycles that ended with the gel reformation at 20 °C. In both cases the amide I′ VCD signal oscillates heavily with time as shown in Fig. 6. For the sample produced by the 20 °C → 50 °C → 20 °C cycle, the oscillations decayed faster than they did for the 5 °C → 50 °C → 20 °C cycle. For 5 °C → 50 °C → 20 °C, the VCD of the final, stable phase is far less pronounced than the corresponding amide I′ VCD of the initially formed phase II gel (Fig. 1 and ref. 23).

The responses of the amide I′ IR band to the annealing cycles does not resemble the behavior of the corresponding VCD signal. For all four annealing protocols we observe a splitting of the broad amide I′ band into two narrower bands. As shown by Farrell *et al.*, the initial gel formation leads to a stronger enhancement of the low wavenumber band (Fig. 1).[23] This is again observed for the reformation process after the 5 °C → 50 °C → 5 °C cycle. The other three reformation processes lead to a more symmetric intensity distribution among the two bands and to broader profiles. The coincidence between peak intensity ratios and the rotational strength of amide I′ modes (*vide supra*) suggest that the former is a measure of the periodicity of the filament/fibril twisting. If filaments exhibit the same or similar pitches over several periods the amide I intensities will be confined to a few excitonic modes.[26]

A peculiarity of how the amide I′ IR band response to the completion of the 20 °C → 50 °C → 5 °C cycle deserves to be highlighted. In the initial phase of reformation at 5 °C, we observed a substantial temporary red-shift of the amide I′ peaks. The low wavenumber amide I′ band position moves between positions that are generally representative of a β-sheet structure (*ca.* 1630 cm^{-1}), and the positions that were observed in the spectrum of gel phase I (*ca.* 1650 cm^{-1}). A concomitant oscillation was observed for the high wavenumber sub-band. At the end of the process these shifts disappear. Interestingly, these redshifts are not accompanied by a drastic change in the VCD spectrum. They complicate the analysis of the amide I′ band profile. To determine how the position and integrated intensity progress over time, we decomposed the IR spectra into Gaussian bands. An example is shown in Fig. S10 (ESI†). Our analysis included bands in the spectral region above 1700 cm^{-1} assignable to the C-terminal CO stretching mode (*ca.* 1720 cm^{-1})[45] and a combination tone of ethanol (*ca.* 1920 cm^{-1}).[46] For our analysis of the amide I′ band profile in the region between 1600 and 1700 cm^{-1}, we allowed band positions to shift over time, contrary to the 'fixed wavenumber' analysis of Farrell *et al.*[23] This turned out to be necessary in order to account for the oscillatory changes of some wavenumber positions (*vide infra*). Fig. S11 (ESI†) shows plots of the integrated intensities and wavenumber positions of the two amide I′ sub-band *versus* time.

For the samples reformed at 20 °C, the amide I′ signals in the VCD spectra exhibit a pronounced oscillation of their amplitude while the corresponding IR spectra change monotonously from one broad to two narrow bands. The respective changes of wavenumber positions and intensities during the reformation process are depicted in Fig. S11 (ESI†).

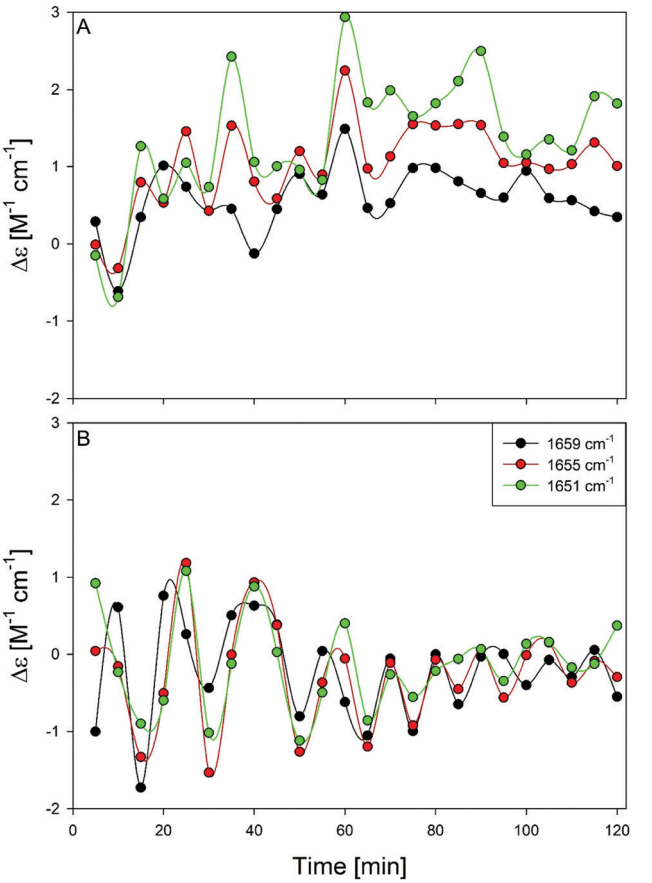

Fig. 6 The vibrational circular dichroism values of GAG/ethanol/water measured at 1651, 1655, and 1659 cm^{-1} *versus* time after completion of an annealing cycle at 20 °C. The annealing cycles were started at 5 °C (A) and 20 °C (B).

One might wonder whether the above results might in part be due to an evaporation of ethanol during the annealing process. To check for this possibility, we determined the integrated intensity of the ethanol combination tone at *ca.* 1920 cm^{-1} and observed no decrease in its integrated intensity over time (Fig. S12, ESI†).

For the reformation of phase I after annealing, the integrated intensities of the amide I′ bands change on a time scale of 20 minutes, which is comparable with the corresponding response time of the initial formation process[23] and faster than the corresponding UVCD kinetics for the 20 °C → 50 °C → 5 °C (Fig. 4a) and 5 °C → 50 °C → 5 °C cycles (Fig. 4b), respectively. No significant wavenumber oscillations were observed for the cycles ending at 20 °C. The intensity changes stretch over a rather long time period of 100 minutes, which is still slightly faster than the UVCD kinetics observed after the 5 °C → 50 °C → 20 °C cycle (Fig. 4b). For 20 °C → 50 °C → 20 °C, the time scales are similar.

Comparing phase I and II reformation

Kinetics of phase II reformation. Farrell *et al.* have shown that the initial formation of GAG-gels at temperatures above *ca.* 18 °C is a comparatively fast process. The VCD of amide I′ is

enhanced by two orders of magnitude and indicative of left-handed helically twisted filaments. Annealing at 50 °C even with a short residence time of 5 minutes changes the formation process of phase II considerably. The differences between initial formation and reformation are particular pronounced in the amide I′ region of the VCD spectrum where the amide I′ signal seem to vary with time in an oscillatory and seemingly chaotic manner. However, a closer look reveals that the changes are by no means chaotic. Fig. 6 shows $\Delta\varepsilon$-values measured at different wavenumbers plotted as a function of time. The individual plots indicate mostly in-phase and out-of phase oscillations of dichroism values with frequencies in the range of between 10^{-4} and 10^{-3} Hz. Higher frequency oscillations seem to be involved in the reformation produced by the 5 °C → 50 °C → 20 °C cycle. The oscillations obtained after the 20 °C → 50 °C → 20 °C cycle seem to be more 'monochromatic' and resembles to some extent a damped oscillator. The most likely explanation for these observations is that the annealing protocol has moved the sample into the region of spinodal fluctuations where filaments are not formed in a continuous way but are rather affected by local density fluctuation which causes the length of filaments to oscillate as well. Such oscillations would have limited influence on the corresponding IR spectrum (Fig. 5) since band positions are becoming length independent if the number of strands in tape exceeds 10.[47,48] VCD variations occur on a much larger length scale.[36] While the reformation of the 20 °C → 50 °C → 20 °C process enters a stable phase after *ca.* 100 minutes, the system did not reach an equilibrium within this time period after the 5 °C → 50 °C → 20 °C annealing. This observation suggests that the initial incubation temperature (and thus the gel phase) does have an influence on the early dynamics of gel reformation. Its influence on the final gel strength is rather limited (*vide supra*), but it is likely that the greater instability of the gel formation phase after the 5 °C → 50 °C → 20 °C cycle is responsible for the slightly lower G_{max}'-value (compared with the kinetics after the 20 °C → 50 °C → 20 °C cycle).

Table 4 lists the time window in which the different phases of the gelation process probed by rheology and the different spectroscopies occur. For the initial formation of phase II the filament formation probed by IR and VCD, the CD-probed dynamics, and the gelation process proceeded on a very similar time scale with the latter proceeding slightly faster than the former.[23] After the 20 °C → 50 °C → 20 °C cycle gel formation the CD kinetics is slightly slower than the filament formation (IR and VCD) and gelation, which are more or less *in sync.* For the 5 °C → 50 °C → 20 °C cycle, however, we observe a fast filament formation (IR/VCD) followed by the CD kinetics and the even slower gelation process.

Table 4 Time interval of kinetic process of GAG reformation after annealing probed by the indicated method

Annealing cycle	Rheology (min)	UVCD (min)	IR (min)
5 °C → 50 °C → 5 °C	10–20	25–50	0–20
5 °C → 50 °C → 20 °C	100–300	50–150	10–80
20 °C → 50 °C → 20 °C	50–100	50–170	40–120
20 °C → 50 °C → 5 °C	4–10	0–15	20
Initial formation T = 5 °C	20–40	0–10	0–10
Initial formation T = 20 °C	0–25	0–20	0–20

Our data for the 20 °C → 50 °C → 20 °C cycle suggest that fibrilization is unstable and progresses further even though the gelation process has already reached a steady state. This interpretation is strongly corroborated by the microscopic images in Fig. 2. They reveal the necessity to complement rheological with spectroscopic experiments for obtaining a complete picture of the dynamics of gel reformation. After 15 minutes the fibrils have grown only from two centers. They overlap, but haven't yet formed the complete space filling network that we observed after 150 minutes. The rheological data in Fig. 3, however, show that G' has already reach nearly 50% of its final value.

Kinetics of phase I reformation. As it can be inferred from the time constants listed in Table 1 the effective times required for gel formation are actually very similar for all three 5 °C → 50 °C → 5 °C reformation cycles (τ varies between 17.7 and 20 min). The time intervals listed in Table 4 suggest that the corresponding fibril formation process probed by the CD kinetics proceeded slower and exhibited a lag time of nearly 25 minutes. However, the filament formation probed by the IR- and VCD responses of the amide I′ mode are faster and level off after *ca.* 20 min, followed by some temporary and always reversible changes of wavenumber positions in the IR spectrum (Fig. 5 and Fig. S11, ESI†). Thus, filament formation and gelation proceed on very similar time scales. This indicates that the formation of filaments is completed at an early state and that the filament state is very stable. The VCD couplet of amide I′ is even larger than that observed after initial formation, which reflect either a higher degree of helicity or longer filaments. The delayed UVCD response indicate that fibrilization into large scale structures is ongoing while the gel is already formed. The final level of UVCD and rheology response to phase I reformation indicates that the reformed gel phase I is substantially stronger than corresponding reformed phase II gels.

Off-pathway aggregation. Our data clearly indicate that a long residence time at 50 °C eliminates the capability of the GAG/ethanol/water sample to reestablish any of the two gel phases. One might be tempted to suspect that this is caused by a complete melting of GAG fibrils and filaments and a dissociation into monomers. However, our data indicate that most of the peptides remain in a somewhat aggregated state even at 50 °C. When the sample is cooled down to either 20 °C or 5 °C after 16 h the still existing peptide aggregates are no longer capable of forming fibrils or even a gel phase. The absorption spectra of samples measured at 50 °C and after the annealing process are remarkably similar to each other and to the corresponding spectra of the gel phases (Fig. S1, ESI†). They exhibit a large redshift from respective band positions in the spectrum of GAG in ethanol/water solutions (Fig. S1, ESI†). Differences between the spectra of phase I and II are quantitative rather than qualitative (the bands are broader for the former). Contrary to what the absorption spectra suggest, the amide I′ profiles in the IR spectra of samples measured after the 20 °C → 50 °C → 20 °C and 5 °C → 50 °C → 5 °C annealing cycles are clearly distinct from the well resolved band structure in the gel spectra. They resemble the amide I′ profile of GAG in ethanol/water mixtures with a high

(40 mol%) ethanol content. The corresponding VCD spectra provide more insights. The amide I′ couplets are an order or magnitude larger than the corresponding signal of GAG monomers in solution, but also an order of magnitude less intense than the strongly enhanced signals of the gel phase. Particularly noteworthy is the fact that the signs of the couplets of the 5 °C and 20 °C spectra still resemble that of the corresponding gel phases (positive and negative, respectively). A first tentative interpretation of all these results can be given by utilizing the results of most recent DFT calculations of Ilawe *et al.*,[26] who geometry optimized several oligomers of GAG in both, implicit water and ethanol, and calculated the corresponding IR and VCD spectra. The shape of the spectra in Fig. 1 very much resemble what these authors observed for pentamers and hexamers of GAG. The rotational strength was underestimated by these calculations, but they yielded an enhancement by a factor 5 over the respective monomer signal, which is very close to the experimentally obtained value. We therefore conclude that the prolonged heating at 50 °C produces a state in which GAG forms the type of disordered oligomers predicted by the DFT calculations of Ilawe *et al.*[26] The corresponding absorption spectra strongly suggest a delocalization of excited electronic states in the oligomers.

We used 50 °C as our annealing process temperature because it is in the middle of the previously reported melting temperature of the system[23] and the evaporation temperature of this water/ethanol mixture. One might suspect, however, that the choice of an higher annealing temperature might have led to a complete dissociation of aggregates into monomers. Therefore, we measured the UVCD kinetics after a 5 °C → 65 °C → 5 °C annealing cycle. As shown in Fig. S13 (ESI†) the amplitude is lower than observed for the corresponding 5 °C → 50 °C → 5 °C cycle, which suggests that lesser on pathway aggregates are available after the completion of the annealing cycle. Looking at the overall kinetics suggests an extended lag time of fibril formation. Interestingly, however, the kinetic trace reached the plateau at the same time as the trace of the 5 °C → 50 °C → 5 °C cycle, which suggest that the reformation after the 5 °C → 65 °C → 5 °C annealing cycle is more cooperative. The corresponding absorption spectrum is shown in Fig. S14 (ESI†). It is still very much diagnostic of GAG aggregates with negligible fractions of monomers. The difference between the molar absorptivities at 221 nm between the absorption spectra obtained after the above annealing cycles does not account for the drop of the $\Delta\varepsilon_{221}$ amplitude.

Why are the oligomers formed after prolonged heating incapable of fibril formation and gelation? At present, we cannot give a definitive answer of this question. We consider it as likely that the initial formation of fibrils and gels is facilitated by a slow dissociation of aggregated GAG after incubation. Instead already existing GAG oligomers or even larger scale aggregates nucleate quickly and form the long fibrils which underlie both gel phases. In other words: peptide aggregation in the solid state enabled on-pathway aggregation with regard to fibrilization and fiber formation after incubation. Heating the sample to 50 °C causes the fibrils to disintegrate into (nearly) amorphous oligomers of limited local order. After a very short residence time at elevated temperatures (several minutes) the number of peptide aggregates are still large enough to reform fibrils and gels of decrease. Over time, however, an equilibrium between different types of oligomers is established that do not have the capability to nucleate and reform fibrils and gel phases. Upon cooling they develop off-pathway into some mildly ordered structures. Interestingly they exhibit some of the chiral character of the fibrils in the initial gel state.

The redshift of the optical bands which persists even after a long residence time at elevated temperatures indicates some strong local interactions between the electronic transitions of individual peptide groups. It cannot be explained by peptide dehydration which should lead to a blueshift of NV1.[49] The single band in the spectrum of monomeric GAG can be assigned to NV1 transition which is generally assumed to arise from a HOMO(π) → LUMO(π^*) transition of the peptide moiety. Corresponding $\pi \rightarrow \pi^*$ transitions of the C-terminal carboxyl group and NV2 transitions of the C═O groups lie outside of our spectral region.[50] It seems that the bands of at least two of these transitions are redhshifted in the optical spectrum of the gel and the unordered aggregates as well. If the redshifts are due to intermolecular electronic interactions these transitions are all likely to be heavily mixed. Our observations resemble to some extent those of Amdursky *et al.*, who reported a pronounced redshift of the phenylalanine bands in the (hydro)gel phase of FmocFF peptides in dimethylsulfoxide/water mixtures, which has been assigned to quantum confinements.[51] Since the spectra in Fig. S1 (ESI†) do not show the characteristic red edge of the FmocFF quantum wells, we do not think that quantum wells have been fully formed in our case. However, the spectra of Amdursky *et al.* clearly show the occurrence of redshifted band even below their critical gel concentration, which is certainly an indicator of the onset of self-assembly which leads to a delocalization of electronic states and transitions.

Conclusion

When first mixed into a subcooled water–ethanol solution, monomeric GAG peptides assemble at water–ethanol interfaces.[37] They promote the formation of a chiral (VCD), long growing fibrils (UVCD) that nucleate from a center nucleus and fans out in all directions. The formed fibrils are of exceptional length (in the submillimeter regime) and form very strong gel phases with the storage modulus exceeding 100 kPa for the gel phase I formed below 15 °C. The size, length, and density of the fibrils depend strongly on the temperature of formation. At T = 50 °C, peptide fibrils quickly dissociate (on a time scale of minutes) to form an ensemble of rather stable amorphous aggregates. If the sample is cooled down below the gelation temperature within the time window of the above decay process, reformation of the gel phases occurs, but the respective kinetic steps are slowed down and the gel strength is reduced while the formation process becomes more cooperative. The corresponding moduli both decrease with the residence time at elevated temperatures as do the amplitudes of the UVCD response, which again appear to be correlated. However, the decrease of the gel strength and the slowing down of gelation kinetics is significantly less pronounced at 5 °C (phase I gel) than it is

at 20 °C (phase II gel). The reformation at 20 °C proceeds through a phase of instability which is likely to involve the rather rapid association and dissociation of filaments. For all reformation processes we observe an ongoing process of fibril formation even after the gel has already reached its maximal storage modulus value. Annealing reduces G'' more than G' which leads to lower values for $\tan\delta$. Cooling after a long residence time (16 h) at 50 °C does not lead to any detectable gelation. However, amorphous aggregates formed at elevated temperature reorganize to some extent in order to form oligomers which reflect the chirality of the initially formed gel phase. Taken together GAG in ethanol/water has emerged as a gel forming system whose strength can be adjusted by the choice of the gel temperature as well as by the residence time of the system at elevated temperature. Both gel phases are kinetically arrested and metastable and their transition into the sol phase should be considered as thermoirreversible. Generally, our results show that even peptides with a low propensity for self-assembly and gelation may form strong gels if the initial conditions (high local concentrations) facilitate the avoidance of the absolute minimum of the Gibbs energy landscape. Hence, the capability of peptides to self-assemble into large scale supramolecular structures should not be solely estimated based on propensities for aggregation.[9] Our results further show that the meta-stable macro fibril structure can be tuned by cycling at elevated temperatures for short time and by choice of formation/reformation temperature. This tunable fibril structure has important implications to the application of GAG peptide fibril gels. For example, microscopy and our analysis of UVCD kinetics clearly show that fewer number of peptides participate in fibril formation with increasing time at high T. Fewer fibril forming peptides decreases the kinetics and strength of gel formation. An additional handle controlling the kinetics and strength of gel is the subcooled formation temperature. By choosing lower temperatures, one induces faster kinetics and a denser fibrillar network which ultimately leads to the formation of stronger gels. A gel's storage modulus is well-known to correlate with a solute's diffusion time by increasing tortuosity within the gel. Changes of the latter affect the release time of drugs which can therefore be modified by changing the gel strength to optimize their efficiency.[52]

Conflicts of interest

There are no conflicts to declare.

Acknowledgements

This project is supported by a grant from the National Science Foundation to R. S. S. and N. A. (DMR-1707770).

References

1 L. Adler-Abramovich and E. Gazit, *Chem. Soc. Rev.*, 2014, **43**, 6881–6893.
2 W. Y. Seow and C. A. E. Hauser, *Mater. Today*, 2014, **17**, 381–388.
3 E. R. Draper and D. J. Adams, *Chem*, 2017, **3**, 390–410.
4 A. R. Hirst, B. Escuder, J. F. Miravet and D. K. Smith, *Angew. Chem., Int. Ed.*, 2008, **47**, 8002–8018.
5 L. J. Dooling and D. A. Tirrell, in *Monographs in Supramolecular Chemistry No 11*, ed. X. J. Loh and O. A. Scherman, Royal Society of Chemistry, London, 2013, pp. 93–124.
6 K. J. Skilling, F. Citossi, T. D. Bradshaw, M. Ashford, B. Kellam and M. Marlow, *Soft Matter*, 2014, **10**, 237–256.
7 A. Nagai, Y. Nagai, H. Qu and S. Zhang, *J. Nanosci. Nanotechnol.*, 2007, **7**, 1–7.
8 P. W. J. M. Frederix, R. V. Ulijn, N. T. Hunt and T. Tuttle, *J. Phys. Chem. Lett.*, 2011, **2**, 2380–2384.
9 P. W. Frederix, G. G. Scott, Y. M. Abul-Haija, D. Kalafatovic, C. G. Pappas, N. Javid, N. T. Hunt, R. V. Ulijn and T. Tuttle, *Nat. Chem.*, 2015, **7**, 30–37.
10 N. Javid, S. Roy, M. Zelzer, Z. Yang, J. Sefcik and R. V. Ulijn, *Biomacromolecules*, 2013, **14**, 4368–4376.
11 R. V. Ulijn, N. Bibi, V. Jayawarna, P. D. Thornton, S. J. Todd, R. J. Mart, A. M. Smith and J. E. Gough, *Mater. Today*, 2007, **10**, 40–48.
12 M. Reches, Y. Porat and E. Gazit, *J. Biol. Chem.*, 2002, **277**, 35475–35480.
13 R. Orbach, I. Mironi-Harpaz, L. Adler-Abramovich, E. Mossou, E. P. Mitchell, V. T. Forsyth, E. Gazit and D. Seliktar, *Langmuir*, 2012, **28**, 2015–2022.
14 G. Colombo, P. Soto and E. Gazit, *Trends Biotechnol.*, 2007, **25**, 211–218.
15 L. Adler-Abramovich, N. Kol, D. Barlam, R. Z. Shneck, E. Gazit and I. Rousso, *Angew. Chem., Int. Ed.*, 2010, **49**, 9939–9942.
16 S. Fleming, P. W. J. M. Frederix, I. R. Sasselli, N. T. Hunt, R. V. Ulijn and T. Tuttle, *Langmuir*, 2013, **29**, 9510–9518.
17 A. M. Smith, R. J. Williams, C. Tang, P. Coppo, R. F. Collins, M. L. Turner, A. Saiani and R. V. Ulijn, *Adv. Mater.*, 2008, **20**, 37–38.
18 S. Marchesan, C. D. Easton, K. E. Styan, L. J. Waddington, F. Kushaki, L. Gooddall, K. M. McLean, J. S. Forsythe and P. G. Hartely, *Nanoscale*, 2014, **6**, 5172–5180.
19 X. Mu, K. M. Eckes, M. Nguyen, L. J. Suggs and R. Rengyu, *Biomacromolecules*, 2012, **13**, 3562–3571.
20 G. Cheng, V. Castelletto, C. M. Moulton, G. E. Newby and I. W. Hamley, *Langmuir*, 2010, **26**, 4990–4998.
21 D. DiGuiseppi and R. Schweitzer-Stenner, *J. Raman Spectrosc.*, 2016, **47**, 1063–1072.
22 B. Milorey, S. Farrell, S. E. Toal and R. Schweitzer-Stenner, *Chem. Commun.*, 2015, **51**, 16498–16501.
23 S. Farrell, D. DiGuiseppi, N. Alvarez and R. Schweitzer-Stenner, *Soft Matter*, 2016, **12**, 6096–6110.
24 C. Diaferia, N. Balasco, D. Altamura, T. Sibillano, E. Gallo, V. Roviello, C. Giannini, G. Morelli, L. Vitagliano and A. Accardo, *Soft Matter*, 2018, **14**, 8219–8230.
25 J. Raeburn, C. Mendoza-Cuenca, B. N. Cattoz, M. A. Little, A. E. Terry, A. Z. Cardoso, P. C. Griffiths and D. J. Adams, *Soft Matter*, 2015, **11**, 927–935.
26 N. V. Ilawe, R. Schweitzer-Stenner, D. DiGuiseppi and B. M. Wong, *Phys. Chem. Chem. Phys.*, 2018, **20**, 18158–18168.
27 N. A. Dudukovic and C. F. Zukoski, *Langmuir*, 2014, **30**, 4493–4500.

28 A. D. Martin, J. P. Wojciechowski, M. M. Bhadbhade and P. Thardason, *Langmuir*, 2016, **32**, 2245–2250.

29 D. J. Pochan, J. P. Schneider, J. Kretsinger, B. Ozbas, K. Rajagopal and L. Haines, *J. Am. Chem. Soc.*, 2003, **125**, 11802–11803.

30 C. Yan and D. J. Pochan, *Chem. Soc. Rev.*, 2010, **39**, 3528–3540.

31 V. V. Pai, P. Bhandari and P. Shukla, *Indian J. Dermatol. Venereol.*, 2017, **1**, 9–18.

32 W. Jentzen, E. Unger, G. Karvounis, J. A. Shelnutt, W. Dreybrodt and R. Schweitzer-Stenner, *J. Phys. Chem.*, 1995, **100**, 14184–14191.

33 S. Jähnigen, A. Scherrer, R. Vuilleumier and D. Sebastinai, *Angew. Chem., Int. Ed.*, 2018, **257**, 1–6.

34 D. Kurouski, R. A. Lombardi, R. K. Dukor, I. K. Lednev and L. A. Nafie, *Chem. Commun.*, 2010, **46**, 7154–7156.

35 S. Ma, X. Cao, M. Mak, A. Sadik, C. Walkner, T. B. Freedman, I. K. Lednev, R. K. Dukor and L. A. Nafie, *J. Am. Chem. Soc.*, 2007, **129**, 12364–12365.

36 T. J. Measey and R. Schweitzer-Stenner, *J. Am. Chem. Soc.*, 2011, **133**, 1066–1076.

37 D. DiGuiseppi, B. Milorey, G. Lewis, N. Kubatova, S. Farrell, H. Schwalbe and R. Schweitzer-Stenner, *J. Phys. Chem. B*, 2017, **121**, 5744–5785.

38 J. Jiang, D. Abramavicius, B. M. Bulheller, J. D. Hirst and S. Mukamel, *J. Phys. Chem. B*, 2010, **114**, 8270–8277.

39 S. Brahms, J. Brahms, G. Spach and A. Brack, *Proc. Natl. Acad. Sci. U. S. A.*, 1977, **74**, 3208–3212.

40 D. DiGuiseppi, B. Milorey, G. Lewis, N. Kubatova, S. Farrell, H. Schwalbe and R. Schweitzer-Stenner, *J. Phys. Chem. B*, 2017, **121**, 5744–5758.

41 K. Rajagopal and J. P. Schneider, *Curr. Opin. Struct. Biol.*, 2004, **14**, 480–486.

42 D. DiGuiseppi, J. Kraus, S. E. Toal, N. Alvarez and R. Schweitzer-Stenner, *J. Phys. Chem. B*, 2016, **120**, 10079–10090.

43 Y. Gao, J. Kim and M. E. Helgeson, *Soft Matter*, 2015, **11**, 6360–6370.

44 T. O. J. Knowles, C. A. Waudby, G. L. Devlin, S. I. A. Cohen, A. Aguzzi, M. Vendruscolo, E. M. Terentjev, M. E. Welland and C. M. Dobson, *Science*, 2009, **326**, 1533–1537.

45 G. Sieler, R. Schweitzer-Stenner, J. S. W. Holtz, V. Pajcini and S. A. Asher, *J. Phys. Chem. B*, 1999, **103**, 372–384.

46 E. Plyler, *J. Res. Natl. Bur. Stand.*, 1952, **48**, 281–286.

47 R. Schweitzer-Stenner, *J. Phys. Chem. B*, 2012, **116**, 4141–4153.

48 C. Lee and M. Cho, *J. Phys. Chem. B*, 2004, **108**, 20397–20407.

49 E. B. Nielsen and J. A. Schellman, *J. Phys. Chem.*, 1967, **1**, 2297–2304.

50 H. D. Hunt and W. T. Simpson, *J. Am. Chem. Soc.*, 1953, **75**, 4540.

51 N. Amdursky, *ChemPlusChem*, 2015, **80**, 1075–1095.

52 Y. Nagai, L. D. Unsworth, S. Koutsopoulos and A. Zhang, *J. Controlled Release*, 2006, **115**, 18–25.

53 W. R. W. Welch, T. A. Keiderling and J. Kubelka, *J. Phys. Chem. B*, 2013, **117**, 10359–10369.